ADVANCED OPTICAL MATERIALS
www.advopticalmat.de

Optical Manipulation of Layer–Valley Coherence via Strong Exciton–Photon Coupling in Microcavities

*Mandeep Khatoniar, Nicholas Yama, Areg Ghazaryan, Sriram Guddala, Pouyan Ghaemi, Kausik Majumdar, and Vinod Menon**

Coherent control and manipulation of quantum degrees of freedom such as spins forms the basis of emerging quantum technologies. In this context, the robust valley degree of freedom and the associated valley pseudospin found in two-dimensional transition metal dichalcogenides is a highly attractive platform. Valley polarization and coherent superposition of valley states have been observed in these systems even up to room temperature. Control of valley coherence is an important building block for the implementation of valley qubit. Large magnetic fields or high-power lasers have been used in the past to demonstrate the control (initialization and rotation) of the valley coherent states. Here, the control of layer–valley coherence via strong coupling of valley excitons in bilayer WS_2 to microcavity photons is demonstrated by exploiting the pseudomagnetic field arising in optical cavities owing to the transverse electric–transverse magnetic (TE–TM)mode splitting. The use of photonic structures to generate pseudomagnetic fields which can be used to manipulate exciton-polaritons presents an attractive approach to control optical responses without the need for large magnets or high-intensity optical pump powers.

1. Introduction

The need for efficient and fast transfer of information has driven a large body of research in the past decade that led to finding alternatives to using moving electrons. Utilizing the spin of the electrons as means of information storage—spintronics emerged as a result of such a quest. But the difficulty in transfer and control of electronic spin and the cryogenic temperatures or complicated sample preparations for maintaining long spin coherence times leave much room for development in this field.[1] Transition metal dichalcogenides (TMDCs) are a class of layered van der Waals (vdW) materials which in addition to various electronic and optical properties like a direct band gap at the Brillouin zone edges (K and K' valleys) and pronounced spin orbit coupling, have come into limelight for their valley selective optical transition rules arising from the breaking of inversion symmetry and their coupling of the layer, valley and spin degrees of freedom.[2]

These valley selective transitions have been exploited to demonstrate valley polarization under circularly polarized pump which excites carriers in either the K or K' valleys[3] and generates valley coherence under linear polarized excitation where both valleys are excited.[4] Valley coherence has received much interest in the context of using the valley pseudospin as a qubit[5] and realizing entanglement between the two valleys when excited with single photons.[6] Till date the manipulation of valley coherence has been achieved either using magnetic fields[7] or using intense optical fields.[8,9] In contrast, here we use the pseudomagnetic field generated in a microcavity to manipulate the valley coherence.

The TMDCs have also become a very attractive platform for studying strong light-matter coupling and exciton-polariton formation.[10] Indeed their valley degree of freedom was exploited in a number of recent works on strong coupling in these low-dimensional systems.[11–14] More recently the enhancement in valley coherence under strong coupling and the control of the valley exciton-polariton propagation was also demonstrated.[15–17] While monolayer TMDCs did show valley coherence, these observations were mostly at low temperature to suppress the undesirable intervalley scattering. In addition to the valley degree of freedom, the 2D TMDCs also offer the layer and spin degrees of freedom.[18,19] The interplay between these degrees of freedom

M. Khatoniar, S. Guddala, P. Ghaemi, V. Menon
Department of Physics
City College of New York
City University of New York
10031 NY, USA
E-mail: vmenon@ccny.cuny.edu
M. Khatoniar, P. Ghaemi, V. Menon
Physics Doctoral Program
The Graduate Center
City University of New York
10016 NY, USA
N. Yama
Department of Electrical Engineering
University of Washington
Seattle, WA 98195-4550, USA
A. Ghazaryan
Institute of Science and Technology Austria
Am Campus 1, 3400 Klosterneuburg, Austria
K. Majumdar
Department of Electrical and Computer Engineering
Indian Institute of Science
CV Raman Rd, Bengaluru, 560012 Karnataka, India

The ORCID identification number(s) for the author(s) of this article can be found under https://doi.org/10.1002/adom.202202631

DOI: 10.1002/adom.202202631

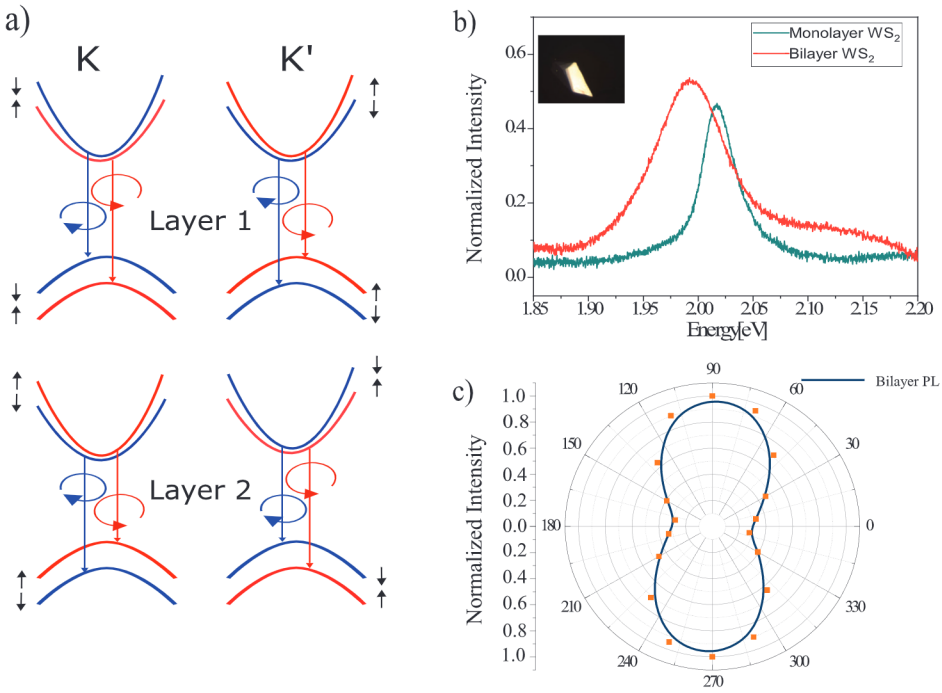

Figure 1. a) Cartoon showing the coherence scheme in bilayer WS_2. b) The normalized white light reflectivity spectrum comparing monolayer and bilayer WS_2 with inset showing optical image of the sample used for the experiment. c) Polarization resolved photoluminescence (PL) of the bilayer sample showing linear polarized emission following the input laser polarization.

results in robust layer-spin-valley coherence which was demonstrated in bilayer TMDCs.[20]

Here we demonstrate the control of layer–valley coherence in bilayer WS_2 via strong coupling of excitons to cavity photons by exploiting the pseudomagnetic field that arises in optical cavities owing to the transverse electric–transverse magnetic (TE–TM) splitting of the cavity photon mode.[21–23]

2. Results and Discussion

Figure 1a is a cartoon showing the electronic bands at K and K' valleys for the tungsten (W) based bilayer TMDC system. Here the helicity dependent optical selection rules get flipped between the two layers as shown by the red and blue transitions in layers 1 and 2 due to their 2H stacking. Although restoration of center of inversion indicates the loss of valley dichroism, the bilayer system retains its spin dichroism as the spin-up and spin-down states are still decoupled owing to the interlayer hopping that conserves spin.[24] This has been realized experimentally in ref. [20] where bilayer WS_2 was shown to retain robust degree of valley polarization and layer-valley coherence even at room temperature.

Bilayer WS_2 was obtained via mechanical exfoliation and were identified using white light reflection as shown in Figure 1b where the absorption from the main exciton (1s) is observed and red shifted compared to the monolayer. After transferring on a quartz substrate linear polarization resolved photoluminescence (PL) measurements were done with a near-resonant excitation of 620 nm using tunable pulsed laser. All measurements were done at room temperature (For details of fabrication and experimental methods—see Experimental Section). The degree of linear polarization (DOP) is defined by $\rho = \frac{I_{max}-I_{min}}{I_{max}+I_{min}}$, where I_{max} is the maximum intensity and I_{min} is the minimum intensity obtained after the PL passes through an analyzer. The value of ρ was obtained by fitting the obtained analyzer angle Θ and normalized intensity I to Malus law, $I = \cos^2(\sqrt{} - \phi) + \frac{1-\rho}{1+\rho}\sin^2(\sqrt{} - \phi)$ with ρ and ϕ (rotation of plane of polarization) as the fitting parameters. For the bilayer sample on quartz cover slip under resonant excitation a value of $\rho = 0.42$ was obtained (Figure 1c) which agrees with previously reported value.[20] Non-resonant excitation at 532 nm shows a lower DOP of $\rho = 0.29$ (see Figure S1a, Supporting Information) due to increased intervalley scattering and electron hole exchange interaction.[25] Valley coherence measurements were also performed on monolayer WS_2 on quartz which yielded a $\rho = 0.14$ (see Figure S1b, Supporting Information) which is low compared to the bilayer. Thus a high degree of coherence retention from the two momentum separated valleys is observed for bilayer WS_2 due to the reduced depolarization mechanisms. This feature, the enhanced layer-valley coherence serves as the main motivation for the use of bilayer WS_2 in the polariton system over monolayers, where one has to go to low temperatures to observe an appreciable degree of valley coherence.[15]

The bilayer WS_2 was encapsulated in an all metal (Ag) mirror cavity with Al_2O_3 and poly(methyl methacrylate) (PMMA) as a spacer layer as shown schematically in **Figure 2**a (See Experimental Section). Figure 2b shows the white light reflection of the encapsulated bilayer. The upper polariton (UP) and lower polariton (LP) branch are fitted to a coupled oscillator model indicated by the green and yellow solid lines, respectively to yield a Rabi splitting of ≈32 meV with a cavity detuning of ≈61.5 meV with respect to the exciton resonance. Polarization resolved PL

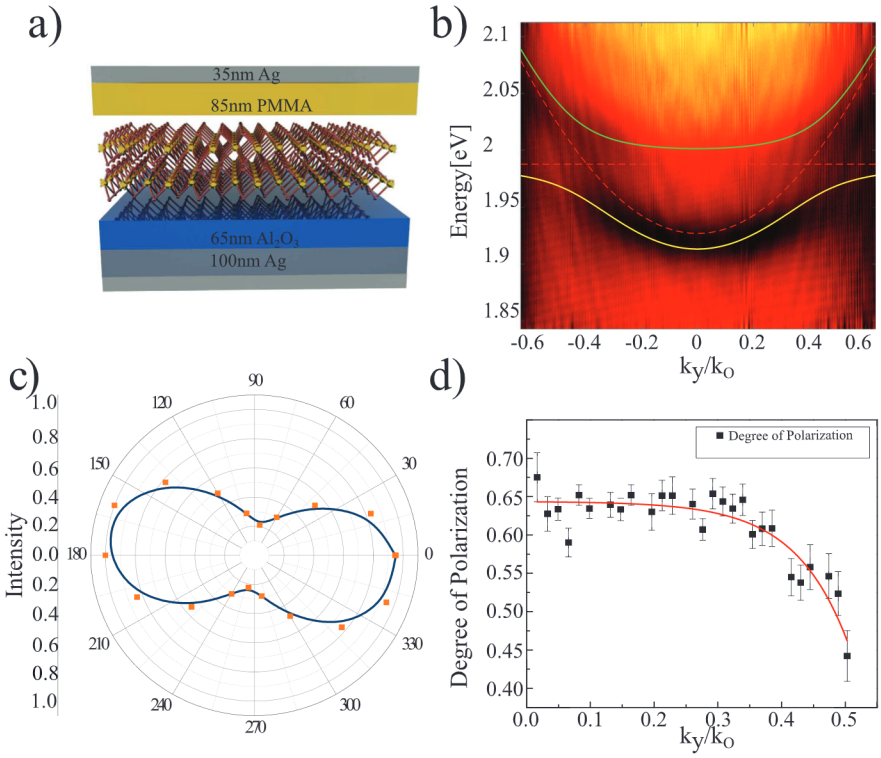

Figure 2. a) Schematic of the cavity structure showing the metal mirror based cavity. b) White light reflectivity of the cavity showing the two dispersion of the two polariton branches. The green and yellow solid lines correspond to the upper and lower polariton branches obtained via coupled oscillator fit. The dashed red lines correspond to the bilayer WS_2 exciton resonance (flat line) and the cavity dispersion (parabolic). c) Polarization resolved polariton photoluminescence (PL) showing linear polarized emission following that of the excitation laser. d) The dependence of DOP on the in-plane wavevector showing a decrease with increasing $k_{\|}$. The error bars indicate the error in the Malu's law fittings.

was mapped in the Fourier space using a 620 nm pulsed laser which is resonant with the UP branch energy at in-plane momentum, $k_{\|} = 0$ (denoted in the figure as k_y/k_0). Here $k_{\|} = \frac{2\pi}{\lambda}\sin\alpha$ with λ, the wavelength and α, the angle made by the incident k (momentum) vector with the normal. The Fourier space PL intensities were binned along $k_{\|}$ ($\Delta k_y/k_0 = 0.02$) to obtain the DOP as a function of in-plane momentum. Figure 2c shows the polar plots with their respective fits at $k_{\|} = 0$. A DOP of $\rho = 0.65$ is obtained for the polariton emission at small in-plane momentum which is higher than the bare bilayer case. This is attributed to the shorter lifetime of the polariton state at small $k_{\|}$. The polariton lifetime at a specific $k_{\|}$ is given by $\tau_k = \frac{\tau_{\text{photon}}}{C_k}$, where τ_{photon} is the lifetime of the photon inside the cavity as determined by it's quality factor and C_k is the photon fraction of the polariton at a given in-plane momentum. At small $k_{\|}$, the photon fraction of the cavity is the highest and hence the lifetime of the polariton is reduced. This process competes with the depolarization processes thereby allowing the polariton to retain a higher degree of coherence compared to that of the bare exciton. A gradual reduction in the DOP as a function of in-plane momentum is observed as shown in Figure 2d. This is attributed to the fact that at large in-plane momentum the lifetime of the polariton increases as the lower polariton branch acquires a higher excitonic fraction. The calculated τ for $k_{\|} = 0$ and $k_{\|} = 0.5k_0$ are 53 and 98 fs, respectively for a cavity with quality factor of 70 as used here. Additionally, the TE–TM splitting becomes significant with increase in $k_{\|}$ which provide an additional polarization relaxation pathway for the polaritons.

Next we demonstrate the manipulation of the plane of polarization with the aid of microcavity. **Figure 3**a shows the schematic of process by which one can realize this rotation in a microcavity taking advantage of the longitudinal–transverse (LT) mode splitting which occurs due to difference in effective path length traversed by the L(TE) and the T(TM) modes inside a microcavity.[21] The presence of LT splitting gives rise to an effective magnetic field (pseudomagnetic field) that goes as $B_x \sim \frac{(k_x^2 - k_y^2)}{(k_x^2 + k_y^2)}$ and $B_y \sim \frac{(2k_x k_y)}{(k_x^2 + k_y^2)}$, where k_x and k_y are the x and y components of the in-plane wavevector k . The presence of this effective magnetic field causes the precession of the polariton pseudospin when initialized with a non zero angle with respect to the magnetic field. The z component of the pseudospin acquired due to the rotation decays as it moves along the Poincare sphere till it is emitted as the polariton decays. And the projection of the pseudospin state on the k_x–k_y plane just before it decays determines it's plane of polarization.[22,26] For this purpose, polarization resolved Fourier image of the entire k-space (k_x–k_y) emission is obtained by removing the slit and letting the entire image fall on the CCD directly, bypassing the grating spectrometer (see Experimental Section). A fixed horizontal input polarization is maintained throughout the experiment. Figure 3b shows the rotation of the plane of polarization as a function of $k_{\|}$. Figure 3c shows

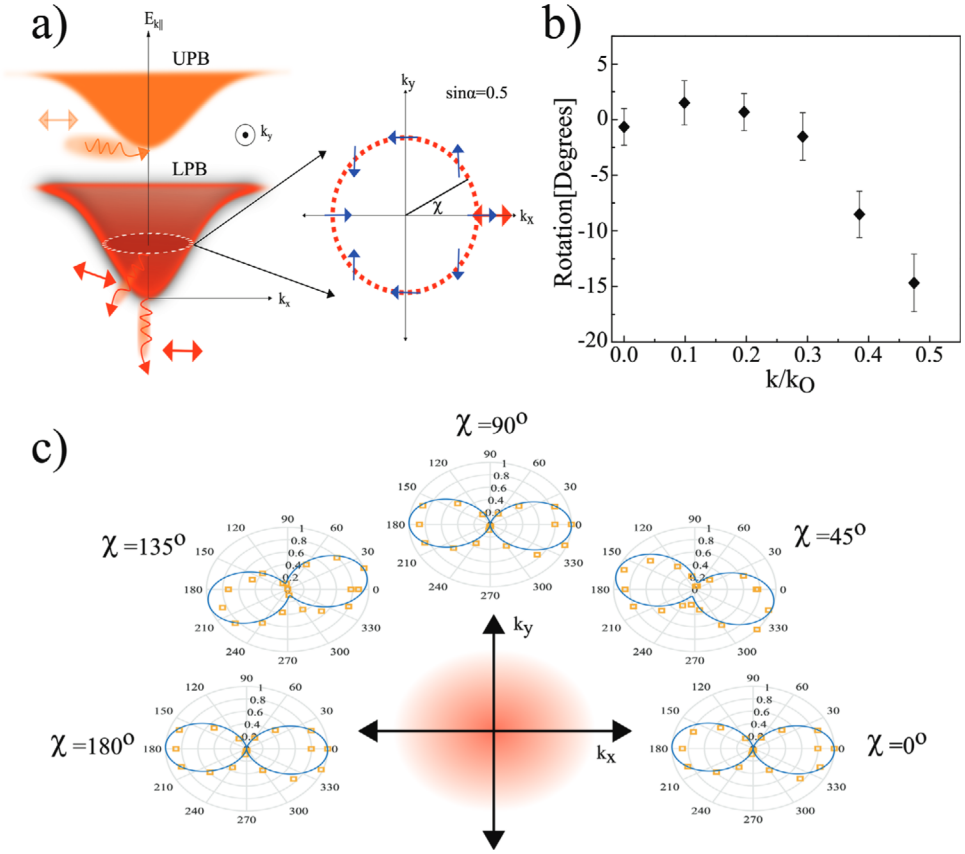

Figure 3. a) Schematic of the experiment used to study the rotation of the plane of polarization. The cavity is excited with a horizontally polarized laser at $k_{\|} = 0$ for the UPB and the rotation of plane of polarization inside the microcavity at a momentum of $k_{\|} = 0.5k_o$ marked by the white dashed circle is measured. The double headed arrow indicates the polarization of the input (orange) and the output PL at different in-plane momentum (red). The direction of the pseudomagnetic field along the *k*-space circle at different in-plane momentum is shown by the blue arrows and the red double headed arrow shows the initialization of the polariton pseudospin . b) The radial dependence of the rotation of polarization ϕ as a function of $k_{\|}$ at a fixed azimuthal angle $\chi_k = 45°$. Error bars indicate the errors due to Malu's law fits. c) The observed rotation of the plane of polarization ϕ as a function of azimuthal angle of the wave vector χ_k with a constant $k_{\|} = 0.5k_0$.

the polar plots of emission intensity as a function of analyzer angle at a fixed value of $k_{\|} \approx 0.5$ for varying azimuthal angle χ. The rotations are limited by the lifetime of the polariton species and the strength of the effective magnetic field. The *Z* component acquired as a result of the precession decays as a function of $\frac{2k_x k_y e^{\frac{-t}{\tau}}}{(k_x^2+k_y^2)}$. As the elastic circle increases with increasing $k_{\|}$ the strength of the pseudomagnetic field increases and thus the *z*-component of of the pseudospin decays faster. Hence we have an upper limit to the range of rotations available. One could change the dielectric environment in the cavity spacer or increase the polariton lifetime using a higher quality factor cavity to increase the extent of rotation.

The polarization dynamics of the polariton states can be described using density matrix formalism.[27] We define the density matrix as $\rho_k(t) = \frac{1}{2}N_k(t) + S_k(t) \times \sigma$ where $N_k(t)$ is the total population of the polaritons in the lower polariton branch. $S_k(t)$ and σ are the pseudospin vector and the Pauli matrix acting on the states excited by the right and left circularly polarized light. Ignoring the hopping between the layers, each layer acts as an independent monolayer of TMD, with valley indices being reversed for the two layers. Therefore, in contrast to monolayer, there is no valley dichroism for bilayer system and specific absorption of circularly polarized light solely corresponds to the spin dichroism close to the band edge.[20,25] Due to the large TE–TM splitting of the metallic cavity and extremely short lifetime of the cavity photon, it is reasonable to assume that the photon population and pseudospin dynamics of the polaritons are determined by their photonic component. Therefore, the dynamics of the population and the pseudospin are governed by

$$\frac{dN_k}{dt} = -\frac{1}{\tau_k}N_k + P_k \tag{1}$$

$$\frac{dS_k}{dt} = -\frac{1}{\tau_{sk}}S_k + \left[\Omega_k^i \times S_k\right] + \frac{P_k}{2} \tag{2}$$

where τ_k is the polariton lifetime as defined previously in the text. $\Omega_k^i = (\Omega_k^x, \Omega_k^y, 0) = \Omega_k(\cos(2\chi_k), \sin(2\chi_k), 0)$ is the pseudomagnetic field due to the TE–TM splitting of the cavity modes $\Delta_{LT}(k)$(i.e., $\Omega_k = \frac{|C_k|^2\Delta_{LT}(k)}{\hbar}$), C_k is the polariton photon fraction and τ_{sk} is the pseudospin lifetime resulting from the decoherence

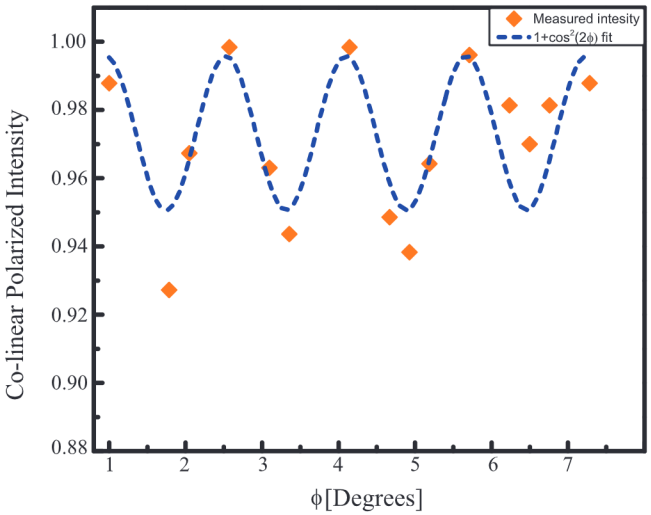

Figure 4. The co-linear intensity as a function of the azimuthal angle χ of the momentum space circle. The orange squares are measured values where the laser polarization and the analyzer are co-linear. The blue line shows a $1 + \cos^2(2\chi)$ dependence as obtained from Equation (5).

mechanisms other than the cavity pseudomagnetic field. χ_k is the azimuthal angle of the momentum $k_{\|}$ and P_k describes the polariton flux initialized by the pump. In the current setup pump is linearly polarized along x-axis thatis$P_k = (P_k, 0, 0)$. In steady state, we get

$$N_k = P_k \tau_k \tag{3}$$

$$S_k^z = \frac{-P_k \tau_{sk}^2 \sin 2\chi_k}{2(1 + {}_k^2\tau_k^2)} \tag{4}$$

$$S_k^x = \frac{P_k \tau_{sk}(1 + {}_k^2\tau_{sk}^2 \cos^2(2\chi_k))}{2(1 + {}_k^2\tau_{sk}^2)} \tag{5}$$

$$S_k^y = \frac{P_k \tau_{skk}^{3\,2} \sin(4\chi_k)}{4(1 + {}_k^2\tau_{sk}^2)} \tag{6}$$

The plane of polarization angle is given by

$$\phi = \frac{1}{2}\arctan\frac{S_k^y}{S_k^x} = \frac{1}{2}\arctan\frac{{}_k^2\tau_{sk}^2 \sin(4\chi_k)}{2(1 + {}_k^2\tau_{sk}^2 \cos^2(2\chi_k))} \tag{7}$$

Figure 4 shows the dependence of the population co-polarized with that of the laser, with a pseudospin corresponding to S_k^x, and angle of rotation of the polarization as a function of the azimuthal angle χ_k. In order to obtain values, close to the experiment, we had to set $\tau_{sk} = 0.9\tau_k$, which indicates that the dominant mechanism of decoherence is the rotation of the pseudospin due to the pseudomagnetic field of TE–TM splitting of the optical cavity. The values of the angle of rotation of polarization are close to the experimentally obtained result, while all three quantities shown in Equations (4)–(6) (see Figure S3, Supporting Information, for plots) perform four full cycles during the 2π change of χ_k. The rotation of plane of polarization ϕ as seen from Equation (7) and Figure S3b, Supporting Information, show that under the current system conditions the maximum rotation available to us is ≈15°. Similar behavior was also reported for AlGaAs quantum well systems at cryogenic temperatures through time resolved spectroscopy of the exciton-polaritons.[26]

3. Conclusion

In summary, we demonstrate room temperature strong coupling of excitons in bilayer WS_2 with cavity photons and the enhanced retention of layer-valley coherence of the polaritons. We exploit the pseudomagnetic field arising from the TE–TM splitting in an optical microcavity to manipulate the polariton layer-valley coherence. The possibility to control the polariton pseudospin by utilizing the pseudomagnetic field generated by the optical anisotropy in cavities presents a hitherto unexplored approach for control of layer-valley coherence in 2D materials via dispersion engineered photonic systems. This presents a promising route to realize active control of valley coherence such as for quantum technologies, where on-demand initialization, rotation, and readout of the valley pseudospin is desirable. Optical cavities and photonic nanostructures with reconfigurable dispersion will be of even greater advantage in this context to realize on demand TE–TM splitting of desired value.

4. Experimental Section

Sample Preparation: Films of bilayer WS_2 were produced via mechanical exfoliation of a single bulk crystal (acquired from HQ Graphene) and identified using photoluminescence and reflectance spectroscopy. The bilayer samples were then transferred, via polydimethylsiloxane stamping, onto a quartz substrate consisting of 100 nm thick silver acting as the bottom mirror with a thin aluminum oxide film of 65 nm deposited via atomic layer deposition serving as the dielectric spacer. The samples were then annealed in argon followed by the deposition of 85 nm PMMA as top spacer layer via spin coating. The microcavity was completed with a 35 nm top layer of silver deposited using electron beam evaporation. Strong coupling was verified using wavevector resolved photoluminescence and reflectance spectroscopy.

Experimental Setup: Optical characterization was performed using a Princeton Instruments Monochromator and PIXIS CCD camera, with excitation from a tunable (500 fs, 80 MHz) pulsed laser (TOPTICA) and the microcavity sample mounted onto an Olympus microscope in reflection geometry. A 50 micron pinhole was placed at the Fourier image plane prior to the sample to block incident light with large in-plane momenta. The output beam was sent through a variable polarizer and lens situated at the Fourier plane, thus resolving the PL in momentum space. In wavelength-k_y resolved spectra for studying in-plane momentum dependence of DOP, a slit along the k_y direction and diffraction grating were used prior to imaging the spectra. In contrast, for full momentum-space images (k_x-k_y) for observation of plane of polarization rotation, the slit and diffraction grating were removed.

Methods of Analysis: The resulting images were then be processed in MATLAB. In case of wavelength resolved images, the intensities of small intervals of k-values (0.02) at the lower polariton emission were summed and averaged. Similarly, for the full k-space images, squares (0.02×0.02) centered at selected points in k-space were summed and averaged. In both cases, the resulting data points were fit to the modified Malus's law equation to determine both the DOP and angle of rotation.

Supporting Information

Supporting Information is available from the Wiley Online Library or from the author.

Acknowledgements

The authors acknowledge insightful discussions with Prof. Wang Yao and graphics by Rezlind Bushati. M.K. and N.Y. acknowledge support from NSF grants NSF DMR-1709996 and NSF OMA 1936276. S.G. was supported by the Army Research Office Multidisciplinary University Research Initiative program (W911NF-17-1-0312) and V.M.M. by the Army Research Office grant (W911NF-22-1-0091). K.M acknowledges the SPARC program that supported his collaboration with the CUNY team. The authors acknowledge the Nanofabrication facility at the CUNY Advanced Science Research Center where the cavity devices were fabricated.

Conflict of Interest

The authors declare no conflict of interest.

Data Availability Statement

The data that support the findings of this study are available from the corresponding author upon reasonable request.

Keywords

2D materials, exciton-polaritons, valleytronics

Received: November 4, 2022
Revised: February 25, 2023
Published online:

[1] S. D. Bader, S. S. P. Parkin, *Annu. Rev. Condens. Matter Phys.* **2010**, *1*, 71.
[2] J. R. Schaibley, H. Yu, G. Clark, P. Rivera, J. S. Ross, K. L. Seyler, W. Yao, X. Xu, *Nat. Rev. Mater.* **2016**, *1*, 16055.
[3] H. Zeng, J. Dai, W. Yao, D. Xiao, X. Cui, *Nat. Nanotechnol.* **2012**, *7*, 490.
[4] A. M. Jones, H. Yu, N. J. Ghimire, S. Wu, G. Aivazian, J. S. Ross, B. Zhao, J. Yan, D. G. Mandrus, D. Xiao, W. Yao, X. Xu, *Nat. Nanotechnol.* **2013**, *8*, 634.
[5] Y. Wu, Q. Tong, G.-B. Liu, H. Yu, W. Yao, *Phys. Rev. B* **2016**, *93*, 045313.
[6] M. Tokman, Y. Wang, A. Belyanin, *Phys. Rev. B: Condens. Matter Mater. Phys.* **2015**, *92*, 075409.
[7] G. Aivazian, Z. Gong, A. M. Jones, R.-L. Chu, J. Yan, D. G. Mandrus, C. Zhang, D. Cobden, W. Yao, X. Xu, *Nat. Phys.* **2015**, *11*, 148.
[8] E. J. Sie, J. W. McIver, Y.-H. Lee, L. Fu, J. Kong, N. Gedik, *Nat. Mater.* **2015**, *14*, 290.
[9] Z. Ye, D. Sun, T. F. Heinz, *Nat. Phys.* **2017**, *13*, 26.
[10] X. Liu, T. Galfsky, Z. Sun, F. Xia, E. Lin, *Nat. Photonics* **2015**, *9*, 30.
[11] Z. Sun, J. Gu, A. Ghazaryan, Z. Shotan, C. R. Considine, M. Dollar, B. Chakraborty, X. Liu, P. Ghaemi, S. Kéna-Cohen, V. M. Menon, *Nat. Photonics* **2017**, *11*, 491.
[12] Y.-J. Chen, J. D. Cain, T. K. Stanev, V. P. Dravid, N. P. Stern, *Nat. Photonics* **2017**, *11*, 431.
[13] S. Dufferwiel, T. P. Lyons, D. D. Solnyshkov, A. A. P. Trichet, F. Withers, S. Schwarz, G. Malpuech, J. M. Smith, K. S. Novoselov, M. S. Skolnick, D. N. Krizhanovskii, A. I. Tartakovskii, *Nat. Photonics* **2017**, *11*, 497.
[14] N. Lundt, P. Nagler, A. Nalitov, S. Klembt, M. Wurdack, S. Stoll, T. H. Harder, S. Betzold, V. Baumann, A. V Kavokin, C. Schüller, T. Korn, S. Höfling, C. Schneider, *2D Mater.* **2017**, *4*, 25096.
[15] S. Dufferwiel, T. P. Lyons, D. D. Solnyshkov, A. A. P. Trichet, F. Withers, G. Malpuech, J. M. Smith, K. S. Novoselov, M. S. Skolnick, D. N. Krizhanovskii, A. I. Tartakovskii, *Nat. Commun.* **2018**, *9*, 4797.
[16] L. Qiu, C. Chakraborty, S. Dhara, A. N. Vamivakas, *Nat. Commun.* **2019**, *10*, 1513.
[17] N. Lundt, Ł. Dusanowski, E. Sedov, P. Stepanov, M. M. Glazov, S. Klembt, M. Klaas, J. Beierlein, Y. Qin, S. Tongay, M. Richard, A. V. Kavokin, S. Höfling, C. Schneider, *Nat. Nanotechnol.* **2019**, *14*, 770.
[18] H. Yu, X. Cui, X. Xu, W. Yao, *Natl. Sci. Rev.* **2015**, *2*, 57.
[19] S. Das, G. Gupta, K. Majumdar, *Phys. Rev. B* **2019**, *99*, 165411.
[20] B. Zhu, H. Zeng, J. Dai, Z. Gong, X. Cui, *Proc. Natl. Acad. Sci. U. S. A.* **2014**, *111*, 11606.
[21] I. A. Shelykh, A. V. Kavokin, Y. G. Rubo, T. C. H. Liew, G. Malpuech, *Semicond. Sci. Technol.* **2010**, *25*, 013001.
[22] O. Bleu, D. Solnyshkov, G. Malpuech, *Phys. Rev. B* **2016**, *96*, 165432.
[23] C. Rupprecht, E. Sedov, M. Klass, H. Knopf, M. Blei, N. Lundt, S. Tongay, T. Taniguchi, K. Watanabe, U. Schulz, A. Kavokin, F. Eilenberger, S. Höfling, C. Schneider, *2D Mater.* **2020**, *7*, 035025.
[24] Z. Gong, G. B. Liu, H. Yu, D. Xiao, X. Cui, X. Xu, W. Yao, *Nat. Commun.* **2013**, *4*, 2053.
[25] K. Hao, G. Moody, F. Wu, C. K. Dass, L. Xu, C.-H. Chen, L. Sun, M.-Y. Li, L.-J. Li, A. H. MacDonald, X. Li, *Nat. Phys.* **2016**, *12*, 677.
[26] W. Langbein, I. Shelykh, D. Solnyshkov, G. Malpuech, Yu. Rubo, A. Kavokin, *Phys. Rev. B* **2007**, *75*, 075323.
[27] I. A. Shelykh, A. V. Kavokin, G. Malpuech, *Phys. Status Solidi B* **2005**, *242*, 2271.